

TECHNICAL ANALYSIS REPORT No: 8/01

OCCURRENCE No: *200100445*

REFERENCE: *BE/200100004*

Examination of a Failed Fan Blade

Rolls-Royce RB211 Trent 892 Turbofan Engine

Boeing 777-300, A6-EMM



EXAMINATION OF A FAILED FAN BLADE ROLLS-ROYCE RB211 TRENT 892 TURBOFAN ENGINE BOEING 777, A6-EMM

EXECUTIVE SUMMARY

On the early evening of 31 January 2001 at Melbourne International Airport, Boeing 777-300 A6-EMM aborted its take-off run at low speed as a result of a failure within the left (No.1) engine. Although the failure was associated with a large compressor surge within the engine, no subsequent fire developed and the aircraft was able to safely return to the terminal building on its remaining serviceable engine.

Failure of the RB211 Trent 892 engine as fitted to the aircraft was a result of the release of a single blade from the low-pressure compressor (fan) rotor disk. The blade release caused extensive damage to the remainder of the fan and the intake shroud, however the event was fully contained. The only escape of debris from the engine was small, low energy fragments, causing minor damage to the fuselage and the opposite engine.

Field and laboratory examination of the released blade found that progressive fatigue cracking had resulted in the loss of two major sections from the blade dovetail root. The remaining material was subsequently unable to carry the centrifugal loads associated with the accelerating engine and failed in ductile shear, allowing the release of the blade from the rotor slot. No defects or other anomalous material or manufacturing features were found to have contributed to the crack development.

The blades installed within the Trent 892-17 engine were an approved variant of the original design, incorporating an undercut radius between the dovetail faces and the blade body. The modification was developed in order to avoid 'edge of bedding' stresses that had been implicated in blade cracking on development engines. Cracking of the released blade had initiated within this undercut radius on both sides of the shear key slot; locations that had been identified by finite element techniques as areas of high localised stress. Extensive galling of the seating surfaces was also found on all blades, indicating the long-term inadequacy of the dry film lubricant applied to the blade dovetail faces. The galling and micro-welding damage can readily interfere with the distribution of loads across the seating surfaces, leading to elevated stresses within the blade root.

Blade failure was thus attributed to an interaction of the following –

- Design – provided for areas of localised high tensile stresses arising from operating loads.
- Operating Stresses – act on the blade to produce cracking in areas highlighted by the design. In the absence of defects predisposing the blade to failure, the development of cracking implies elevated operating stress levels.
- Blade – Disk Connection Problems – galling of the dovetail surfaces indicates the potential for uneven load distribution through the connection, leading to increased stresses within the blade root and thus a greater disposition to fatigue cracking.

EXAMINATION OF A FAILED FAN BLADE ROLLS-ROYCE RB211 TRENT 892 TURBOFAN ENGINE BOEING 777-300, A6-EMM

FACTUAL INFORMATION

Introduction

This report addresses specifically the technical aspects of the failure of the aircraft's engine. Air safety occurrence report No. 200100445 references this document.

On the early evening of 31 January 2001 at Melbourne International Airport, Boeing 777-300 A6-EMM aborted its take-off run at low speed as a result of a failure within the left (No.1) engine.

The failure was reported by the flight crew as being characterised by a single loud 'bang' and the immediate left yaw of the aircraft. A flash of flame from the engine intake and other short lived visual indications of fire were observed by passengers and air traffic controllers, however no fire warnings were received on the flight deck.

Following the rejection of the take-off, the left engine was immediately shut down. After assessment from ATC and the attending fire-fighting services to confirm the absence of fire, the aircraft was able to return to the terminal on its remaining serviceable engine.

Engine Failure

Event

Passenger video footage captured the moment of engine failure and showed a large burst of flame and bright white sparks escaping from the engine intake as the aircraft accelerated. The event was coincident with the loud 'bang' reported by the flight crew. Attachment A presents a series of frames captured from the footage and shows the development of the event.

Fan Failure

The initial inspection of the left engine intake and cowl areas (figure 1) revealed extensive damage to the fan and the adjacent shroud and intake linings (figures 2 & 3). A single blade was entirely missing from the rotor disk and the adjacent blade behind this had lost roughly one-half of its outer length (figure 4). The remainder of the blades showed severe trailing edge and tip damage. Extensive damage and destruction of the fan shroud extended a considerable distance forward and behind the blade path (figures 5, 6 & 7). Sections of the aluminium housing along the fan track were torn away, exposing areas of the underlying acoustic insulation (figures 8 & 9).



Figure 1 (Left) Intake of the failed engine.

Figures 2 & 3 (Centre) General view of the damage inflicted to the intake cowl and fan.

Figure 4 (Bottom Left) Fan rotor showing the position of the released blade and the damage to the trailing blade.

Figure 5 (Bottom Right) Blade debris embedded within the intake cowl.



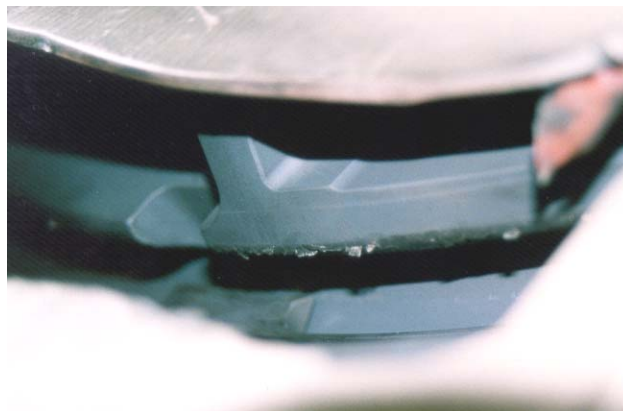


Figure 6 (Top L) Stripping of the cowl lining, exposing the honeycomb matrix.

Figures 7 & 8 (Top R, Above) Typical damage experienced along the fan track.

Figure 9 (Right) Internal area of shroud impact by the released blade.

Inspection of the rotor disk showed the complete release of the blade, with only the blade slider plate remaining within the dovetail slot (figure 10). The annulus filler plate on the concave side of the blade slot was intact and in place – the plate on the convex side had fractured at its mid-point, with the loss of the rear section. The forward edges of the disk slot on the concave side showed an irregular ridge of material raised from the inner face (figure 11).



Figures 10 & 11 Fan disk slot showing damage to the annulus fillers and slot edges.

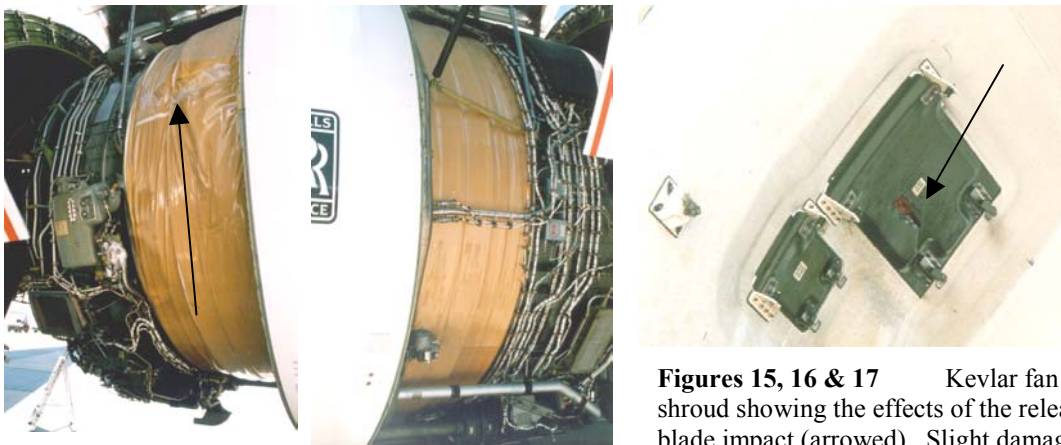
A considerable amount of large debris had accumulated immediately behind the fan, including the heavily damaged liberated blade itself (figures 12 & 13). The vanes around the engine core inlet showed prominent impact damage along the leading edges (figure 14) and suggested the ingress of material into the low-pressure compressor section.



Figures 12, 13 & 14 Debris accumulated behind the fan (including the liberated blade). Damage also shown by the core intake vanes.

Containment

Examining the external surfaces of the kevlar containment shroud showed a single outward bulge at roughly the 9.00 o'clock position (figures 15 & 16). Perforation of the shroud was not evident around this area, although minor damage to the inside cowl surface (figure 17) and the hinges had occurred, necessitating repair. The mounts to the engine oil reservoir had broken and the body of the tank was cracked and leaking. All pipes and hose-work were intact.



Figures 15, 16 & 17 Kevlar fan shroud showing the effects of the released blade impact (arrowed). Slight damage also to the interior of the cowl opposite the impact area.

Evidence around the aircraft suggested the escape of a small amount of debris from the engine intake during the failure. The left side of the fuselage, adjacent to the engine showed two small perforations where liberated debris had impacted (figure 18). A small fragment of blade material was recovered from the larger of these perforations (figure 19). In a similar way, the right engine of the aircraft showed evidence of foreign object ingress, with a 15mm long chip in the leading edge of a single blade (figure 20). Tearing of material from the fan track and the acoustic panels behind the fan was also noted (figures 21 & 22).

The majority of the debris produced by the engine failure was ejected from the rear of the engine and distributed along a path biased toward the left side of the runway. The debris make-up was consistent with the materials found within the fan and intake components of the engine (figure 23).

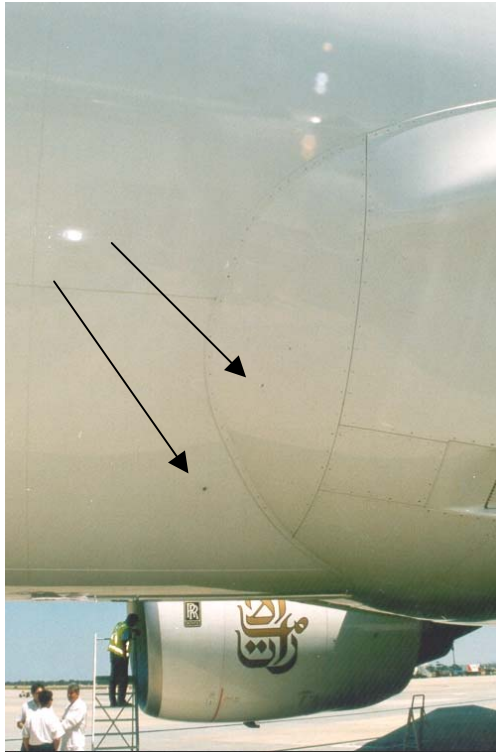


Figure 18 (L) Locations of fuselage damage from released debris.

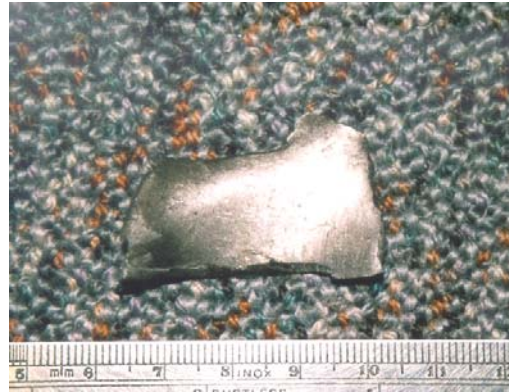
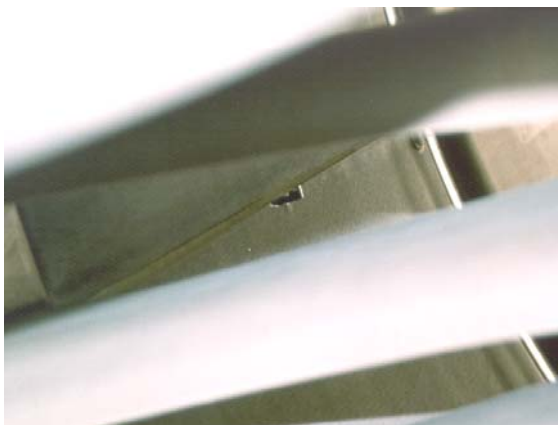


Figure 19 (Above) Debris fragment removed from the fuselage.

Figures 20, 21 & 22 (Below L&R, Bottom L) Damage to the intake and a blade of the right (No. 2) engine.

Figure 23 (Bottom R) Typical debris as recovered from the runway surface.



Blade Release

The fractured blade was extracted from behind the fan and laid out for preliminary study. Roughly fifty percent of the outer length had been torn away at an angle downward from leading to trailing edges (figure 24) and an appreciable length of the convex surface had folded backward upon itself. The dovetail root of the blade was missing two considerable sections along the convex edge at either side of the shear key slot (figure 25). Both areas showed a similar curved crack front and both appeared to have originated from the undercut region between the face of the blade and the dovetail upper surface (figures 26 & 27). Of the two large sections that were lost through final separation from the blade base, one was recovered from the collected debris, together with a smaller section of blade base, the shear key, slider plate and chocking spring (figure 28).



Figure 24 (Top L) Released blade as recovered from the engine cowl.

Figure 25 (Top R) Dovetail root of the released blade showing the loss of two large sections.

Figures 26 & 27 (Centre) Appearance of the fractured blade root sections located on either side of the shear key slot.

Figure 28 (Left) Segments of the released blade and other mounting components as recovered from the released debris.

Engine

The failed No. 1 (left) engine of the aircraft was identified as a Rolls-Royce RB211 Trent, model 892-17, serial number 51197. According to information from the operator, the engine had operated for 5,765 hours and through 907 cycles before the failure – all of which was on aircraft A6-EMM. A review of the maintenance history for the engine showed no record of defects or maintenance actions associated with the engine fan or associated assemblies.

Blade

The fractured blade was number nine within the rotor disk, which contains twenty-six of these items. The blade was identified as serial number *RGG16936*, which was part of fan set number 691194. The blades were of unsupported wide-chord design, produced as a diffusion-bonded and forged sandwich of Ti6Al4V wrought titanium alloy plate. Identification marks on the underside of the blade root were photographed and transcribed as follows:

FK30842ASSY
 S/N-RGG16936
 USN RRTOT
 1 98
 78.1
 32.1
 66.1S-TIP
 P93.3 TAN
 N55.8 AX
 11663.0



Assembly Components

The shear key, slider plate and chocking spring from the failed blade assembly were recovered from the disc slot and ejected debris. These items were intact, however all had experienced mechanical damage consistent with the nature of the failure. The items were identified as follows:

Slider Plate	Shear Key	Chocking Spring
M29561 RALB55 FK 22216 ASSY 108G	FK23918 WN 21028/55 FMBB7	FK 1063 M26950 RALB31
<i>In another area:</i>		
FK22217 M26862 RALB31		

TECHNICAL EXAMINATION

Primary Failure

The recovered fan blade was returned to the ATSB's Canberra facility for in-depth examination and analysis by the Technical Analysis unit. Prior to removal of the root region to facilitate closer study, the remains of the blade were weighed to assess the material loss and to allow calculations by the manufacturer of the blade behaviour during the failure sequence.

- Main Segment 7,650 g
- Root Piece 122 g
- Edge Piece 14 g

- Original Blade Mass 11,663g

- Material Lost 3,876g

The fracture surfaces were manually mapped to illustrate the relative sizes and dimensions of the fractured regions and to establish a basis for the assessment of crack development (attachment B). Following this, the blade was sectioned using cooled abrasive techniques to remove the fractured root (figure 30) and reduce it to suitably sized sections for cleaning and closer study (figure 31).



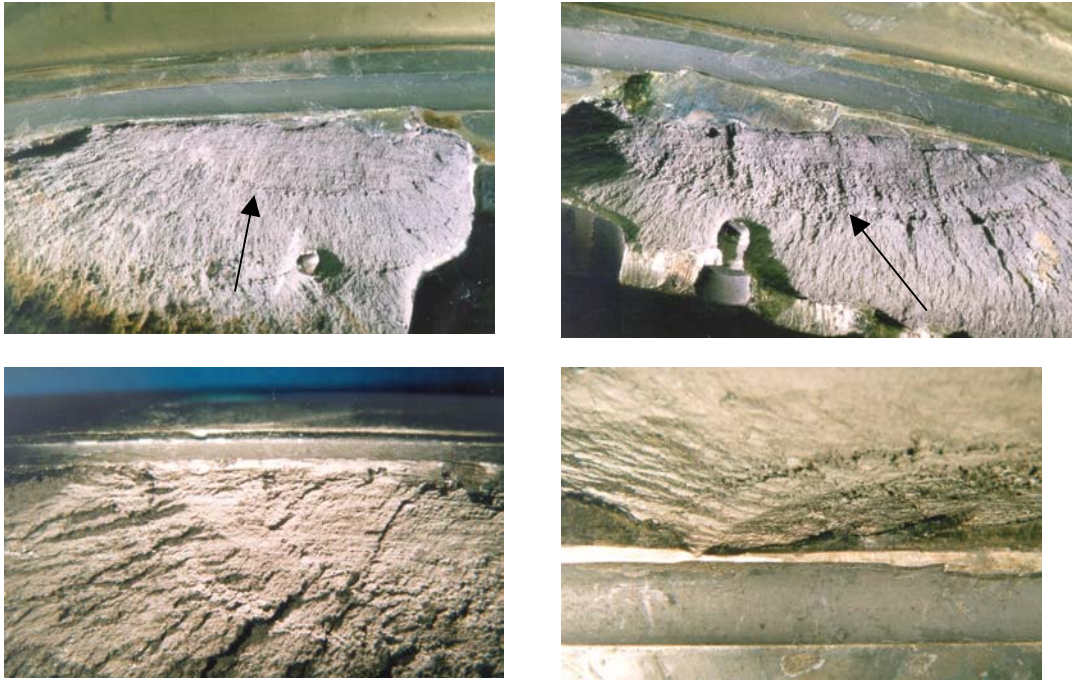
Figures 30 & 31 Preparatory sectioning of the blade to facilitate laboratory examination.

Visual Fractography

Cracking had developed in adjacent locations on either side of the shear key slot on the concave side of the blade. Each had initiated from a region on the undercut radius, estimated at roughly one-third the way around the circumference from the edge of the dovetail face. In both cases the initiation site/s had been extensively damaged by impact and yielded little information of significance.

The fracture surfaces in general were characterised by a zone of fine, fibrous fracture surrounding the origins and extending into the section in a semi-circular fashion. The subsequent transition to a slightly rougher surface with no fibrous features was clearly defined, with this zone extending inward to the limits of the fractured segments, which were often surrounded by regions of bright ductile shear. Within the inner zone of cracking were several narrow, clearly defined arrest marks; each surrounding the

regions of initiation (figures 32 & 33). Closer examination between the inner and outer fracture zones illustrated the presence of many finer arrest marks leading out to the transition area (figures 34 & 35) – clearly highlighting the change in fracture behaviour at this point.



Figures 32 & 33 (Top) The pattern of fatigue crack progression is clearly highlighted in both areas. The point of change in crack propagation mode is arrowed.

Figures 34 & 35 (Bottom) Both figures show the arrest marks associated with cyclic crack propagation. Note the dramatic increased in arrest mark separation beyond the inner region of cracking.

Examining the surfaces of the undercut radius confirmed the presence of a shallow layer of dry film lubricant. Spalling and flaking of this layer had occurred alongside the fracture, exposing the underlying material, which had the typical dimpled appearance of a shot-peened surface (figure 36). Aside from the induced mechanical damage, no features of a detrimental nature were noted along this area on either side of the blade.



Figure 36 Undercut radius region at the region of crack initiation. Note the dry lubricant film spalling and the ‘dimpled’ metal undersurface, typical of shot peening.

Scanning Electron Microscopy

Characterisation of the fracture mode and surface features of both areas of cracking was conducted under the scanning electron microscope. The distinctive appearance of the crack arrest marks and the transition in fracture morphology were identified easily at low magnifications (figure 37).

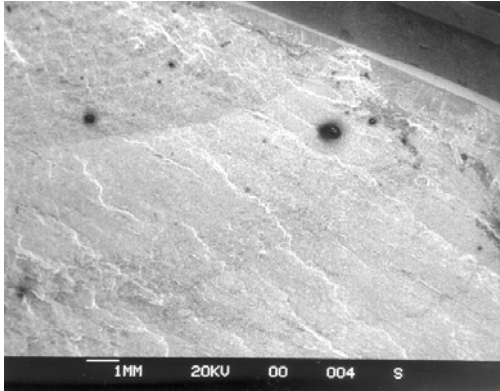


Figure 37 (L) Shows the increase in arrest mark separation at the transition between HCF and LCF crack propagation.

Within the inner region surrounding the damaged initiation sites, the surface was dominated by faceted, transgranular fracture with no evidence of striation (figure 38). These features were also evident to a lesser extent within each of the arrest bands extending away from the central area. Beyond the limit of faceted crack growth, features more indicative of tensile overload fracture dominated the surface. A mixture of dimpled ductile failure and remnant transgranular cleavage was evident in most locations (figure 39).

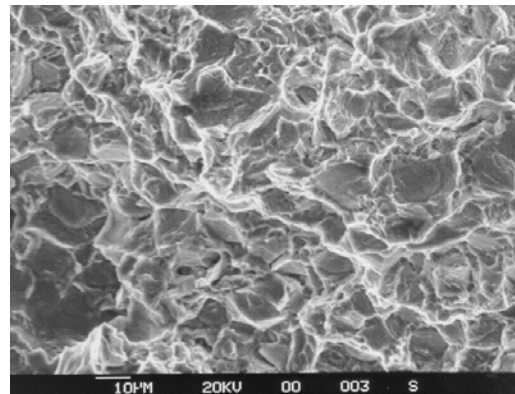
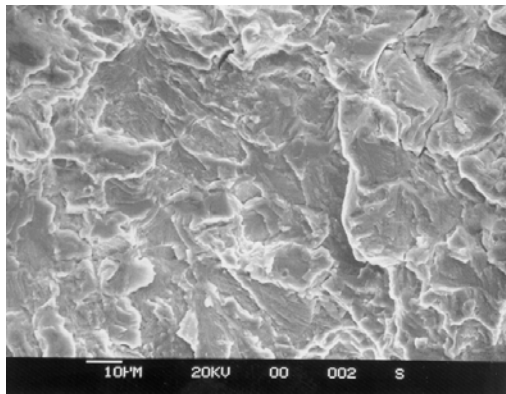


Figure 38 (L) Area of fracture near the point of origin, showing flat, faceted propagation with no defined striations (typical of HCF).

Figure 39 (R) Area of fracture towards the final failure – much more ductile appearance consistent with the higher tensile stresses experienced at this stage of cracking.

All observations showed no evidence of material or manufacturing defects that may have contributed to crack initiation.

Other Blades

The opportunity was made available to inspect the slightly damaged blade from the No. 2 (right) engine of A6-EMM (figure 40). Aside from the localised impact damage to the leading edge (figure 41), the aerofoil surfaces of the blade were free from other anomalous features.

The dovetail surfaces of the blade on both the concave and convex sides showed an appreciable degree of galling and micro-welding type damage (figures 42 & 43). The transverse orientation of the damage was consistent with the effects of seat sliding and bedding under centrifugal loads. The dry film lubricant (grey coating) that had been present over the surfaces had broken down and become discontinuous in the seating areas and had allowed intermittent metal-to-metal contact between the disc and blade dovetail faces.

Inspection of other blades from both engines showed the seat galling damage to be consistent throughout the fan assemblies of both engines.



Figures 40 & 41 (Top) Damaged blade from the right engine, showing only the single leading edge nick.

Figures 42 & 43 (Bottom) Significant galling damage to the dovetail mating surfaces. Remnant dry film lubricant is present (dark grey regions), however galled areas are intermixed with this along the full blade length.

Material Analysis

Chemical Analysis

A sample of the failed blade material was analysed by spectrographic techniques and returned the following composition.

Ti	Al	V	Fe	Ni	Cr	Co	Mo	Cu	Zr	C	Sn	Ru	Nb
Bal	5.64	4.05	.17	<.01	.01	<.01	<.01	<.01	<.01	.01	<.01	<.01	<.01

This result meets the general commercial specification for UNS R56400 titanium alloy (Ti6Al4V). The levels of Carbon and Iron impurities measured within the sample are within the specification requirements of low impurity grade UNS R56401 (Ti6Al4V-ELI).

Metallographic Examination

A suitably sized micro-section was taken through the fracture surface and convex side radius areas of the failed blade and prepared for metallographic study. The presence of dry film lubricant on the external surfaces was confirmed and was measured to a thickness of around 40µm adjacent to the dovetail face. A shallow surface layer of flattened and distorted grains was also noted around the radius – consistent with the effects of machining and/or shot peening (figure 44). The root radius in general was smoothly machined, with no apparent physical or microstructural surface discontinuities (figure 45).

Studying the general structure of the blade root revealed a fine distribution of equiaxed α grains within a matrix of β and coarse acicular α (figure 46). Anomalous microstructures were not evident.

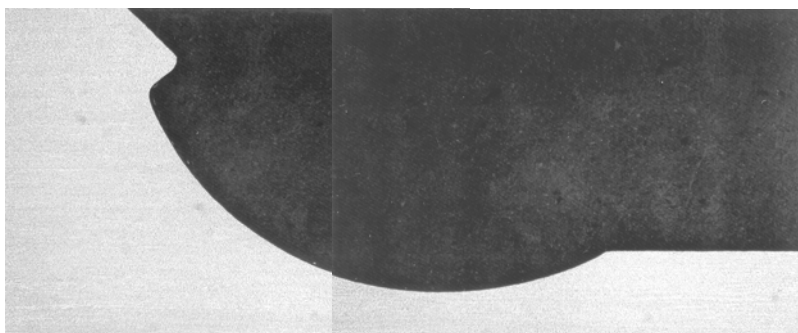
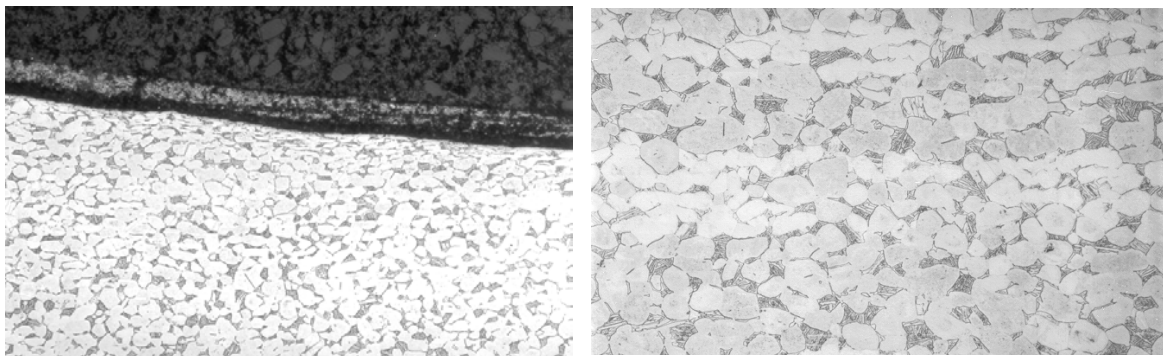


Figure 44 (Top L) Microstructure of a section taken through the undercut radius (X200).

Figure 45 (Top R) Typical microstructure of the blade root block (X400)

Figure 46 (L) Profile of the undercut radius adjacent to the cracked areas (X13).

Hardness Tests

Conventional Vickers hardness tests were carried out on a suitably prepared cross-section through the root radius. Material approximately 5mm below the radius surface and adjacent to the fracture path returned hardness values within the range of 327 – 339 HV₁₀.

Stress Analysis

Finite element modelling of the Trent 892 undercut blade was carried out by the manufacturer under steady tensile and vibratory stress conditions. This work showed the maximum tensile stresses to be present under steady state conditions, with the stresses concentrated about the undercut radius at either side of the shear key slot. Attachment C presents the stress distribution diagrams for both sides of the blade.

These areas of highest stress were coincident with the locations of crack initiation on the convex side of the failed blade.

ANALYSIS

Failure Event

The description of the failure event from the flight crew and the images captured by the passenger video footage were both consistent with a large compressor surge being associated with the blade release. The interruption of airflow through the engine core produced by the blade release was expected to be the main factor in the development of the surge. The bright white sparks accompanying the burst of flame from the engine intake are characteristic of titanium materials and thus indicative of major disruption of the rotating fan at this time.

Blade Manufacture

Analysis and testing of the failed fan blade confirmed its production from a Titanium – Aluminium – Vanadium alloy. While a specification for the blade material was not received from the manufacturer, the alloy did comply with the general elemental composition for a UNS R56400 alloy (Ti6Al4V), which is commonly employed in fan blade applications. The root area alloy hardness of around 330 HV was also within the range typically expected for alloys and components of this nature. Microstructurally, the blade showed no anomalous structures or defects that were contributory to the failure, although the obliteration of the crack origins during the blade release prevented any further investigation in this regard.

A study conducted by the blade manufacturer examined all relevant aspects of the blade's production history. The conclusion reached from this exercise was that the released blade (S/No: RGG16936) was a typical production standard Trent 800 fan blade (P/No: FK30842).

Failure

The release of the fan blade from the disk slot resulted from the cracking and loss of physical support offered by the dovetail root section on the convex (suction) side of the blade. Cracking had developed at either side of the shear key slot and had grown into the root section under a fatigue mechanism, typified by the radiating pattern of progression marks on the fracture surfaces. The initial growth of fatigue cracking to a depth of around 10 – 12mm had occurred with no distinguishable striations and presented a woody, fibrous fracture that mimicked the directional, banded nature of the wrought parent metal microstructure. At magnification, the surface showed a faceted form with no obvious ductility. These features were consistent with the development of cracking under a high-cycle, low stress regime (HCF), whereby the crack propagation path is dominated by microstructural morphology, producing the features observed. The absence of definable striations prevented an assessment of crack growth rates, however the closely spaced arrest marks that became observable towards the limits of this region were considered to represent individual flight cycles.

The abrupt transition of fracture morphology to a much more ductile appearance was considered to represent the transition to a low-cycle, high stress crack propagation mode (LCF). Crack propagation over this area was much more rapid, with only two or three definable flight-cycle arrest-marks identified over the surface to the point of final failure.

SUMMARY

From the factual information and examination findings, several principal factors contributing to the development of the blade failure were identified.

- **Blade Design.** The direct correlation between the areas of highest design stresses and the areas of crack initiation suggests that the failure was primarily a response of the blade design to the applied stresses. It also indicates that isolated defects or other anomalous features, if present, were not influential in the failure.
- **Operating Stresses.** In conjunction with the above, the magnitude and nature of the stresses placed on the blade were also of significance in the failure. The initiation of fatigue cracking requires exposure to a finite number of stress cycles, with the number of cycles required being inversely proportional to the level of stress. Failure at a disproportionately low number of cycles thus implies the exposure of the component to an elevated level of cyclic stress.
- **Dovetail Surface Galling.** The presence of significant levels of galling and micro-welding between the blade and fan-disk load bearing surfaces indicates an increase in friction between the surfaces and a breakdown of normal sliding contact. The dry lubricant film applied to the blade dovetail surfaces had proven ineffective in preventing the galling damage. The design of the blade-to-disk connection relies upon the uniform and even seating of the blade within the disk slot as the fan revolves. The connection is such that increases in engine speed (and hence centrifugal blade loads) will produce sliding movement and pressure across the dovetail faces as the blade beds deeper into the disk slot. In the presence of irregular galling, the blade loads will not be evenly carried through the dovetail connection, with the potential localised overstressing of the section and the development of cracking as experienced.

CONCLUSION

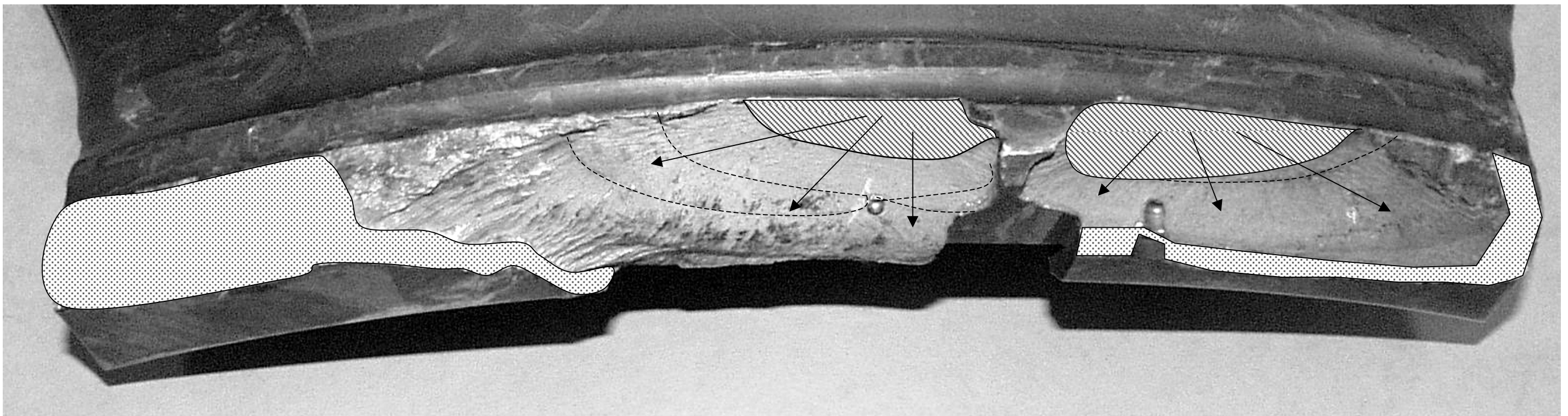
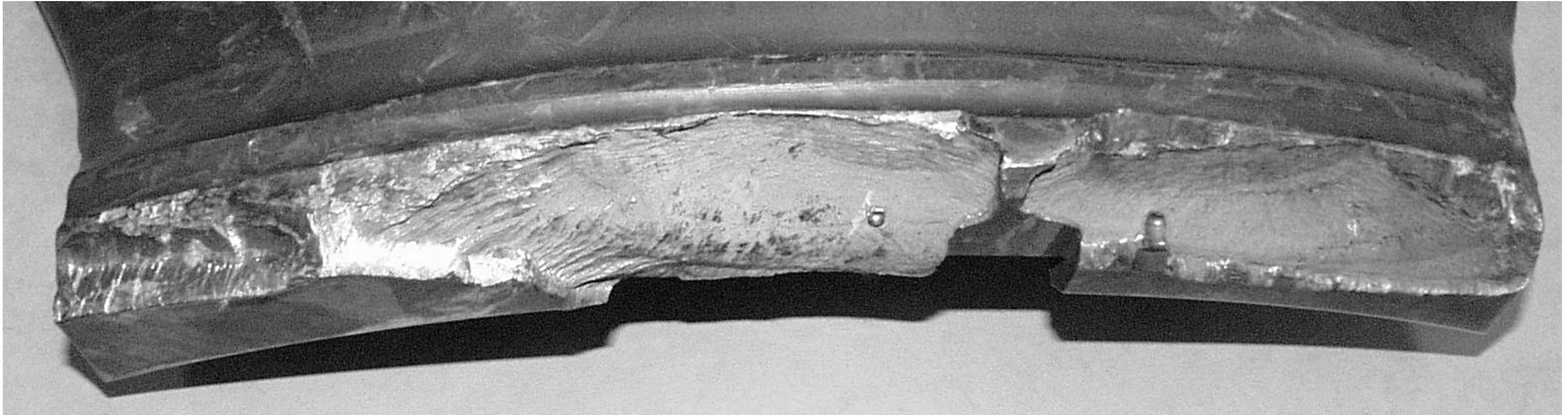
Findings




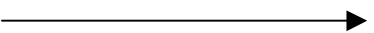
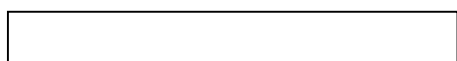
1. The engine failed as a direct result of the loss of a single low-pressure compressor (fan) blade.
2. The failure was contained.
3. Release of the blade occurred due to the initiation and growth of fatigue cracking within the convex root of the component.
4. The blade was free from any material or manufacturing defects that could have influenced the failure.
5. The development of fatigue cracking was attributed to the synergistic effects of extended periods of high power operation and uneven blade root seating.
6. The uneven blade root seating stemmed from the breakdown of the dry-film lubricant layer between the load bearing surfaces, allowing irregular surface galling and micro-welding damage to accumulate.
7. B777-300 aircraft operating in hot, dry environments typically require extended periods of high power operation in order to meet the specified performance requirements. The operations of aircraft A6-EMM were typical of this.

Attachment A. Sequential images of the engine surge event associated with the blade release.

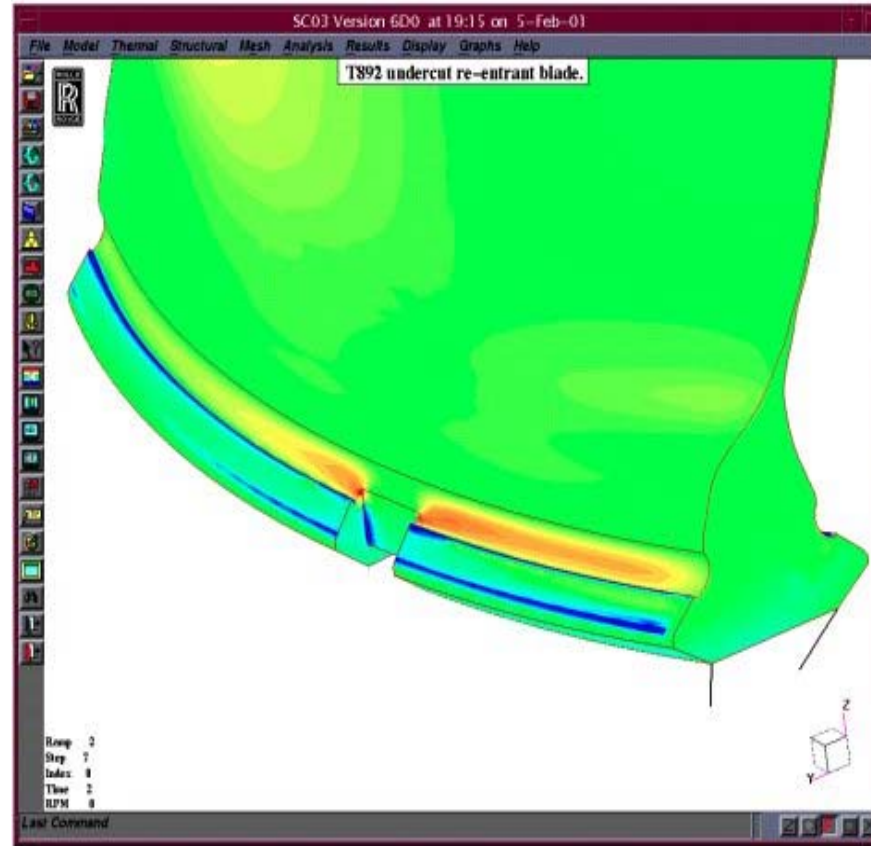
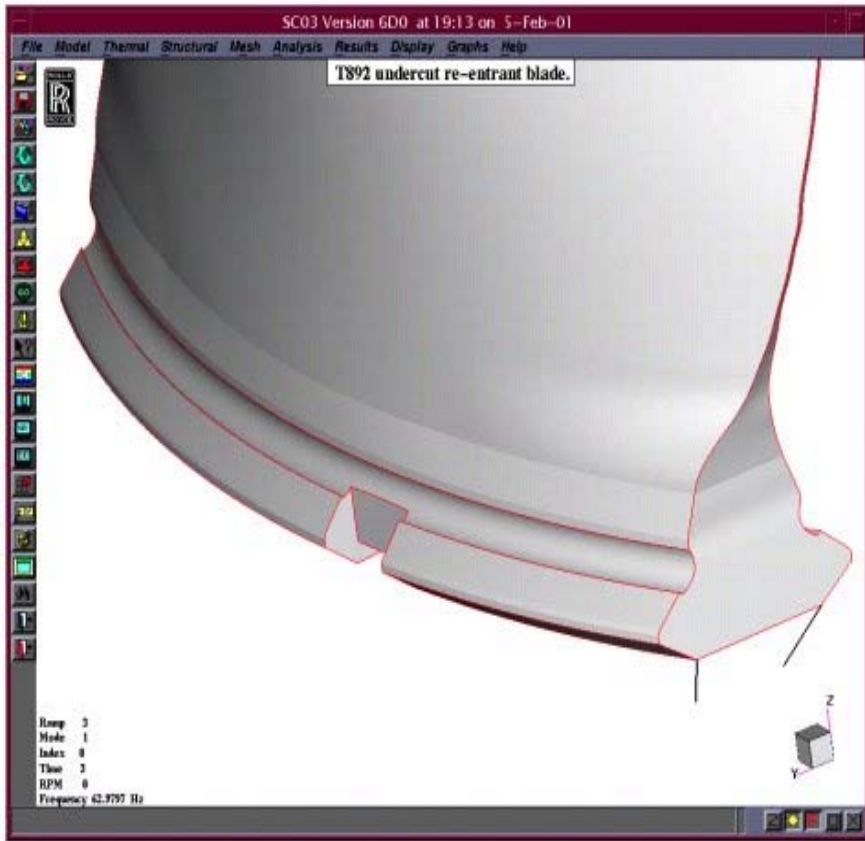


Attachment B. Image map illustrating the significant fracture regions.

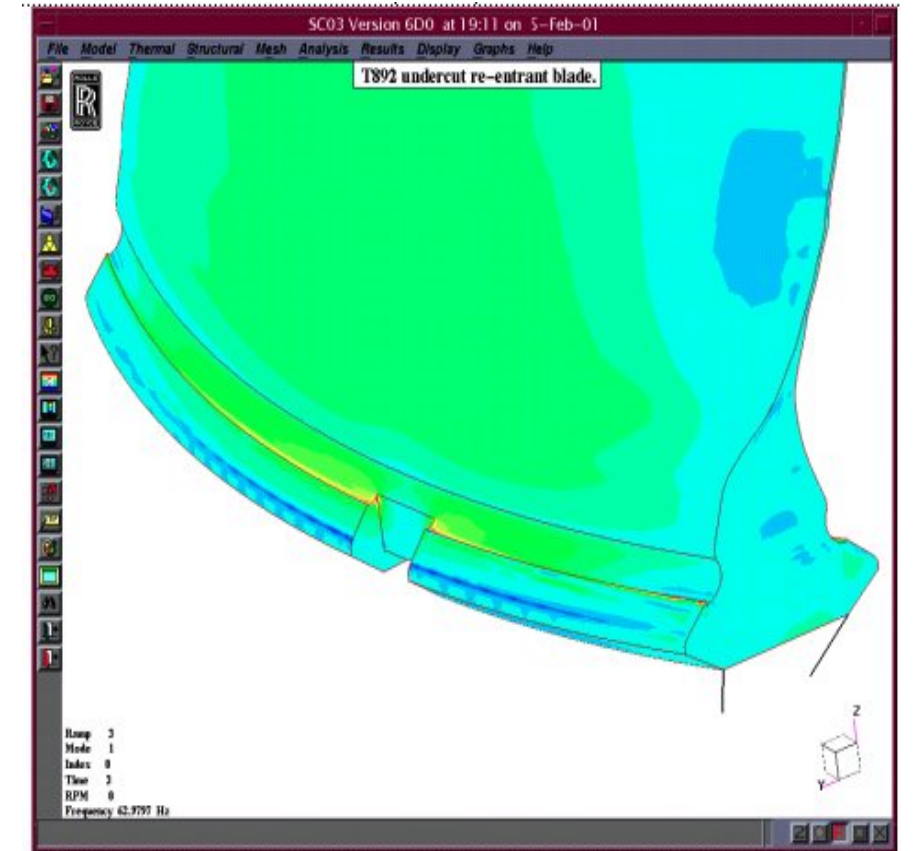


	Area of HCF Fatigue Cracking	Crack arrest marks	
	Area of final ductile overload fracture	Direction of crack propagation	
	Area of LCF fatigue cracking		

Attachment C. Finite element stress analysis plots for both direct tensile stress and vibratory stress conditions. Peak tensile stresses are shown in red, peak compressive stresses in blue.



Stress distribution under static tensile loads ↓↑



Stress distribution under vibratory loads ↓↑

